ORIGINAL ARTICLE

Assessing glass-ceramic homogeneity and nucleation self-correlation by crystallization statistics

María Helena Ramírez Acosta[1] [ID] | **Lorena Raphael Rodrigues[1]** [ID] |
Edgar David Guarin Castro[2] [ID] | **Edgar Dutra Zanotto[1]** [ID]

[1]Graduate Program in Materials Science and Engineering, Department of Materials Engineering, Federal University of São Carlos, São Carlos, Brazil

[2]Department of Physics, Federal University of São Carlos, São Carlos, Brazil

Correspondence

María Helena Ramírez Acosta, Graduate Program in Materials Science and Engineering, Department of Materials Engineering, Federal University of São Carlos, São Carlos, São Paulo, Brazil.
Email: churimahe@hotmail.com

Funding information

Coordenação de Aperfeiçoamento de Pessoal de Nível Superior—Brasil (CAPES), Grant/Award Number: 001; National Council for Scientific and Technological Development (CNPq), Grant/Award Number: 141057/2017-3 and 141816/2018-0; São Paulo State Research Foundation, Grant/Award Number: 2013/07793-6

Abstract

In this work, we implemented and tested a statistical method to evaluate the microstructural uniformity of partially crystallized glasses employing the aggregation index (*R-index*), a parameter derived from the Poisson distribution function, which has mainly been used in Ecology studies. Since the crystal nucleation rate strongly depends on the chemical composition, the spatial crystal distribution in glass-ceramics can be used to infer their *chemical homogeneity*. We also tested the hypothesis, advanced by some authors, of preferential *secondary* nucleation close to preexisting crystals (even in chemically homogeneous samples). To this end, we conducted a nearest-neighbor statistical analysis of the spatial crystal distribution in partially crystallized $Li_2Si_2O_5$ and $Ba_5Si_8O_{21}$ glasses, used as model materials, by inspecting optical micrographs obtained at different magnifications. The resultant *R*-indexes indicate a very high degree of homogeneity of the crystal number distribution, reflecting the uniform distribution of the chemical elements in the parent glasses. Moreover, the results for both glasses refute the suggestion that crystal nucleation is self-correlated. These outcomes allow us to suggest the *R*-index as a valuable and easily implemented tool to evaluate the chemical homogeneity of glasses that undergo internal nucleation, such as those used for glass-ceramics.

KEYWORDS

chemical homogeneity, glass-ceramic, nearest-neighbor index, nucleation, poisson distribution

1 | INTRODUCTION

A system is considered spatially homogeneous regarding one or more of its properties when they are invariant with respect to the spatial location. In the design of high-performance glasses and glass-ceramics, chemical homogeneity is a valuable, desirable property, allowing for the reproducibility of optical, mechanical, thermal, electrical, and other characteristics, regardless of the analyzed portion of the material. Furthermore, most theoretical models of nucleation kinetics (e.g., the Classical Nucleation Theory, CNT) assume a chemically homogeneous material. Therefore, any crystallization analyses of vitreous materials would be incomplete without preliminary inspection of their chemical homogeneity.

To access the chemical homogeneity of glasses, optical[1–4] and chemical[5,6] procedures have been proposed. However, since all these methods have some limitations, chemical homogeneity determination is still a current challenge. Such limitations include inconsistent results of optical methods based on the Christiansen-Shelyubskii procedure,[7,8] and the difficulty in obtaining, interpreting, and getting an accurate estimate of the elemental composition due to the considerable amount of spectra generated by chemical methods,[9] such as laser-induced

breakdown spectroscopy (LIBS)[5] and laser ablation inductively coupled plasma mass spectrometry (LA-ICP-MS).[6] Even though these chemical methods could determine if a given glass is homogeneous, the lowest spatial scale is limited by the laser spot size, generally of several microns. Consequently, some alternative methods[10–15] have arisen; among them, the one proposed by Souza et al.[12] is particularly interesting as it enables the quantification of chemical homogeneity of glasses and the associated scale in a practical way. This is accomplished indirectly by a statistical analysis of the spatial crystal distribution in partially crystallized glasses.

In this work, we follow a similar procedure to that proposed in Souza et al.[12] However, instead of using only the number of crystals, the present method compares the departure of an experimental spatial crystal distribution from an equivalent random, uniform distribution of reference by comparing the mean nearest-neighbor distances between both distributions. The reference distribution is based on the Poisson point statistics since it describes the complete spatial randomness of a discrete random variable,[16] such as the number of crystals distributed in different areas of a specimen. Then, the homogeneity degree and the scale at which the observed spatial crystal distribution departs or approaches a random expectation can be quantified by the aggregation index (R). An advantage of this method over that reported in Souza et al.[12] is the possibility of determining the system tendency towards clustered or periodic crystal distributions, in addition to its homogeneity degree and scale. The R-index was proposed long ago by Clark and Evans[17] for Ecology applications. Nevertheless, its mathematical foundation is valid for the statistical analysis of any objects that can be treated as "points" distributed in any mathematical space (e.g., line, area, or volume), such as the distribution of crystals in a glassy matrix (glass-ceramic).

Hence, this article's first objective is to test, for the first time, the R-index method to evaluate the chemical homogeneity of glasses that can be crystallized internally, such as those used for glass-ceramics. Its goal also is to verify if the standard laboratory practice of melting, crushing, and remelting *twice* leads to chemically homogeneous glasses. Finally, we also intend to test whether a recent suggestion of preferential nucleation that leads to the formation of satellite-like crystals near previously existing crystals[18] (nucleation self-correlation) is valid for oxide glasses. Bearing in mind these objectives, we present in the following sections the theoretical background associated with the R-index (Section 2), the methodology to test its validity in partially crystallized $Li_2Si_2O_5$ and $Ba_5Si_8O_{21}$ glasses, used here as model materials (Section 3), and the main results (Section 4). To conclude, we discuss the method's reliability and its advantages for determining the chemical homogeneity degree in glasses that undergo internal nucleation in experimental time scales (Sections 5 and 6).

2 | SPATIAL ANALYSIS OF POINT DATA

2.1 | Point spatial distributions

The distribution of a certain number of points in space can tend toward agglomeration, uniform randomness, or periodicity, as shown respectively in Figure 1A–C, for the particular case of a two-dimensional (2D) space.[19]

The precise identification of these patterns is relevant since it could give clues about the underlying process or the physical interactions that originate them. In general, if there are preferential regions, they will lead to agglomerated (Figure 1A) or periodic (Figure 1C) point spatial distributions, respectively.
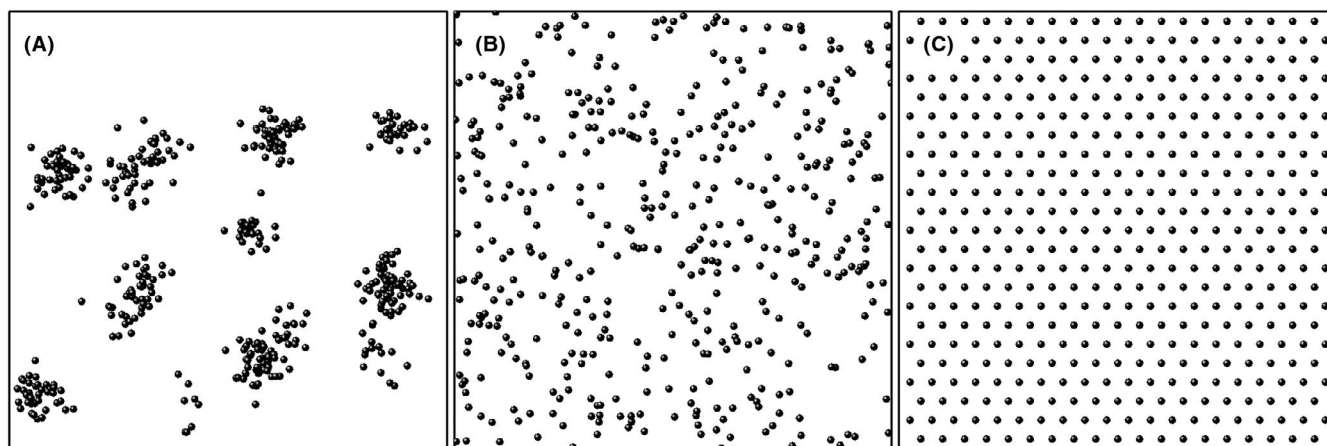

FIGURE 1 Simulated (A) clustered, (B) uniform random, and (C) periodic 2D point distributions. Each distribution contains 448 points in a square of 100×100 arbitrary units. The simulations that resulted in these figures were carried out using the Matplotlib[36] and Scikit-learn[39] Python libraries

On the other hand, the absence of any preference in the system induces uniform random patterns (Figure 1B). Randomness or stochasticity is the main characteristic of phenomena that varies unpredictably or are guided by chance. Mathematically, randomness is defined as a collection of random variables (N) indexed by a mathematical set (T), which could be time (t) or space (s), such that $\{N(t): t \in T\}$ or $\{N(s): s \in T\}$. In other words, at every t or s in set T, a random number $N(t)$ or $N(s)$ is observed.[20] Uniform random distributions are particularly interesting for the statistical analysis of point distributions because they can be used as a reference or null models to characterize other point patterns, which are generally more common in nature.[19]

2.2 | Crystal nucleation and Poisson point process

Crystal nucleation in glasses is a stochastic phenomenon, characterized by a crystalline nuclei random appearance in a vitreous matrix.[21] This process occurs at any temperature below the melting point, after a certain time.[22] The crystal nucleation process is distinguished as homogeneous or heterogeneous. In the former case, two properties are satisfied at different regions of the analyzed system, observed at any scale: (i) the crystal number density is independent of the area scrutinized, and (ii) the emergence of a nucleus is independent of any other. Property (i) reflects the fact that there are no preferential sites for crystal nucleation in the vitreous matrix, whereas property (ii) indicates that crystallization in one region does not influence crystallization in another one. This is true for the so-called stoichiometric or polymorphic crystallization when the chemical composition of the parent glass and crystal are the same. For glass formers that present internal nucleation, with or without the addition of nucleating agents, these conditions are only reached in a chemically homogeneous glass. Consequently, one can expect a uniform random crystal distribution, similar to the point pattern displayed in Figure 1B.

On the other hand, heterogeneous nucleation starts at preferential sites, such as foreign solid particles and surfaces—cracks, bubbles, or phase boundaries—which locally decrease the thermodynamic barrier.[23] Fluctuations of chemical elements inside the vitreous matrix also generate nonuniform crystal distributions. Some factors producing these fluctuations could be an incomplete mixture of the chemicals before melting; the high viscosity of the glass-forming melts,[12] which impairs mixing; and the use of reagents with a high-density difference (e.g., barium or lead silicates). In addition to chemical inhomogeneity, nucleation forming periodic distributions (Figure 1C) can be obtained by local and guided heat treatments, using, for instance, laser-induced crystallization.[24]

In the case of nonuniform crystal distributions, such as clustered (Figure 1A) or periodic (Figure 1C) dispositions,

the property (ii) is not satisfied. This situation can occur, for instance, by preformed crystals that favor the formation of satellite-like crystals around them, as hypothesized in a recent study,[18] or by controlling the appearance of crystals in specific locations inside the glass matrix by a local laser heat treatment, such as in photo-thermo-refractive glasses.[25,26] On the other hand, clustered systems usually do not obey property (i) because the crystal number density tends to vary when analyzing equal areas in different system regions or changing the analyzed areas' size. Conversely, periodic systems exhibit a constant crystal density at different regions of the system with the same area and at different subareas, complying with the property (i).

Since the spatial crystal distribution in a partially crystallized sample reflects the parent glass's chemical homogeneity, statistical analysis can be used as an indirect measurement of homogeneity. Thus, the spatial distribution of crystals should satisfy properties (i) and (ii) to guarantee it results from a homogeneous glass, that is, the probability to find a crystal in such uniform distribution should be characterized by a Poisson distribution function. This function describes the distribution of a set of points randomly disposed on a mathematical space where an event is independent of others.[16] For a 2D crystal random distribution, the probability (P) of finding a certain number of crystals (N) in a specific area (A), is given by[16]:

$$P\{N(A) = n\} = \frac{\overline{N}^n}{n!}\exp^{-\overline{N}}, \tag{1}$$

where the number of crystals is a nonnegative integer, such that $N(A) = n$, with $n = 0, 1, 2, \ldots$, $\overline{N} = \rho A$ is the mean number of crystals in a specific area, and ρ is the number of crystals per unit area.

2.3 | The nearest-neighbor index, R

Hertz[27] and Clark and Evans[17] showed independently that in a population of objects following a Poisson distribution in a 2D space, Equation (1), the probability of finding the nearest neighbor at a distance r from a reference point, located at the center of a circular area, is given by the Weibull probability distribution function, defined as follows[17]:

$$P(r) = 2\pi\rho r e^{-\rho\pi r^2}, \tag{2}$$

with a mean or expected value $\overline{r}_E = 1/\left(2\sqrt{\rho}\right)$ and a standard deviation $\sigma_{\overline{r}_E} = 0.26136/\sqrt{N\rho}$. Thus, based on the Poisson and the Weibull distributions, Clark and Evans[17] proposed the aggregation index (R-index) to establish the degree of departure from uniform random expectation of an observed distribution. The R-index compares the mean value of the nearest-neighbor

distance ($\bar{r}$) in an observed point distribution with the mean value of the nearest-neighbor distance that would be expected ($\bar{r}_E$) if that distribution was random. The R-index is then defined as:

$$R = \frac{\bar{r}}{\bar{r}_E}, \qquad (3)$$

whose variance is given by $\text{var}(R) = 0.2732/\bar{N}$.[28] R takes values between 0 and 2.149. The lower limit ($R = 0$) corresponds to perfect agglomeration, where all the objects have the same coordinates, then $\bar{r} = 0$. Correspondingly, if R is small, the distribution of points looks like the clustered pattern shown in Figure 1A, where $R = 0.49$ (as will be shown in Section 4.1). The upper limit ($R = 2.1491$), on the other hand, indicates perfect periodicity, corresponding to a hexagonal point distribution inside a hexagonal region, where the distance between points is maximized,[17] as roughly represented in Figure 1C. However, if the observed distribution is perfectly uniform, random, and homogeneous, similar to the distribution shown in Figure 1B, $\bar{r}$ equals $\bar{r}_E$, and $R = 1$.

3 | MATERIALS AND METHODS

3.1 | Glass preparation

Lithium disilicate ($Li_2Si_2O_5$) and pentabarium octosilicate ($Ba_5Si_8O_{21}$) glasses were selected for this study because both undergo internal nucleation in laboratory time scales when properly heated, allowing for statistical analyses of crystal distributions in partially crystallized samples. The $Ba_5Si_8O_{21}$ glass was synthesized from $BaCO_3$ (Alfa Aesar, 99.8%) and SiO_2 (Vitrovita, >99.9%). The reagents were previously homogenized in a Turbula T10B mixer and calcined at 1653 K for $BaCO_3$ decomposition and the formation of the phase of interest. Then, the mixture was melted in a Pt crucible at 1793 K for approximately 30 min. To enhance the chemical homogeneity, the liquid was quenched, broken, and remelted twice and finally poured and pressed between two steel plates to form ~3-mm-thick glass samples. The $Li_2Si_2O_5$ glass was not previously calcined but was prepared using the same melting/splat cooling process; the full procedure is described in Deubener et al.[29]

3.2 | Heat treatments

Samples of approximately $3 \times 3 \times 3$ mm^3 were partially crystallized following double-stage heat treatments in vertical furnaces with a precision of ± 1 K. This method consists of heating the samples to the nucleation temperature (T_n) and keeping them during a nucleation time (t_n). After

TABLE 1 Double stage heat treatments used to partially crystallize the $Li_2Si_2O_5$ and $Ba_5Si_8O_{21}$ glasses

Composition	T_n (K)	t_n (min)	T_d (K)	t_d (min)
$Li_2Si_2O_5$	708	3780	865	10
	745	450		15
$Ba_5Si_8O_{21}$	948	300	1085	8
	988	10	1103	5

that, the samples are cooled back to room temperature and then treated at a development temperature (T_d) for a time t_d, to grow the nuclei previously formed at T_n until a detectable size.[30] All the information about the heat treatments used in this work is summarized in Table 1. These heat treatment cycles were selected to make the observation of crystals in the samples' cross-section feasible in the selected optical magnifications.

3.3 | Microstructural analysis

To observe the crystal distribution in the samples' cross-section using reflected light optical microscopy, the partially crystallized samples were initially ground using 320 to 1200 grit SiC paper and polished with a CeO_2 solution. Afterward, $Li_2Si_2O_5$ samples were immersed in a room-temperature ultrasonic water bath for ~10 min at a frequency of 37 kHz, whereas $Ba_5Si_8O_{21}$ samples were etched in a 2% HF (vol%) solution for ~10 s to reveal the crystals. Since the homogeneity degree can change when analyzing different spatial scales of the same system, the study of the crystal spatial distribution was performed using three optical magnifications for each sample. The micrographs were obtained using a Nikon Eclipse LV 100 N Pol microscope with a coupled camera DS–fi2. For the $Li_2Si_2O_5$ glass, magnifications of 200×, 500×, and 1000× were used, whereas, for the $Ba_5Si_8O_{21}$ glass, magnifications of 500×, 1000×, and 1500× were employed. The criterion to choose these magnifications was the facility in visualizing and counting crystals, due to moderate nucleation rate of each glass, whose maximums are ~10^9 m^{-3} s^{-1} for the $Li_2Si_2O_5$ glass[30] and ~10^{12} m^{-3} s^{-1} for the $Ba_5Si_8O_{21}$ glass.[31,32]

To ensure a statistically representative number of micrographs, we estimated that a minimum number of ~385 crystals should be counted for each magnification. This number was obtained using a sample size calculator,[33] considering a confidence level of 95%, a margin of error of 5%, and an unknown population of crystals. Thus, a total of 12, 17, 18, and 19 micrographs were taken for magnifications of 200×, 500×, 1000×, and 1500×, respectively. All micrographs were analyzed with the software ImageJ[34] to determine the number of crystals (N), and the Cartesian

coordinates (x, y) of the crystals' geometric centers. This information is necessary to access the parameters $\bar{r}$, $\bar{r}_E$ and, consequently, the R-index as will be explained in the next sections.

3.4 | Edge correction and nearest-neighbor distance calculation

When a subarea of a 2D point distribution is analyzed, edge effects should be considered to reduce the overestimation of the mean nearest-neighbor distance, and consequently, the R-index. The edge effect emerges due to the presence of points outside the studied region that cannot be accounted for in the calculations, albeit they can be nearest-neighbors of points close to the edges and inside the observed area.[35] To minimize this effect, in our analysis, we implemented an edge correction procedure, namely, NN1 (nearest-neighbor 1), proposed in Pommerening and Stoyan.[35] The strategy consists of filtering all the crystals close to the micrographs' edges, whose distances to their nearest-neighbors are greater than their distances to one of the analyzed area edges. Otherwise, the points will not be discarded. As a result, a new 2D distribution with N' crystals is obtained, such that $N' \leq N$.

For example, let us consider a simulated distribution of 399 points randomly distributed in a unit area,[36] as presented in Figure 2A. Now, let us take a smaller area near the top edge, containing two points P_1 and P_2, with their respective nearest neighbors P_1^{NN} and P_2^{NN}, as shown in Figure 2B. The distance from P_1 and P_2 to their nearest neighbors are r_1 and r_2, respectively. In this case, the distance, a_1, from P_1 to the top edge is less than r_1 ($a_1 < r_1$). Consequently, P_1 will be discarded by the edge correction procedure. In contrast, the distance a_2 from P_2 to the top edge is greater than r_2 ($a_2 > r_2$). Therefore, P_2 will not be discarded since P_2^{NN} is most likely to be its nearest-neighbor.

Knowing the Cartesian coordinates (x, y) for each point in the original distribution, the above-described conditions can be checked for every point. Figure 2C displays the 31 discarded open green circles and the new set of $N' = 368$ particles, enclosed by a new area (blue square), which is smaller than the original. This new area is defined by tracing a rectangle whose edges pass close to the four outermost particles (red triangles) of the new particle set. Figure 2D shows one of the four outermost points, P_0 (red triangle), with its nearest-neighbor (black
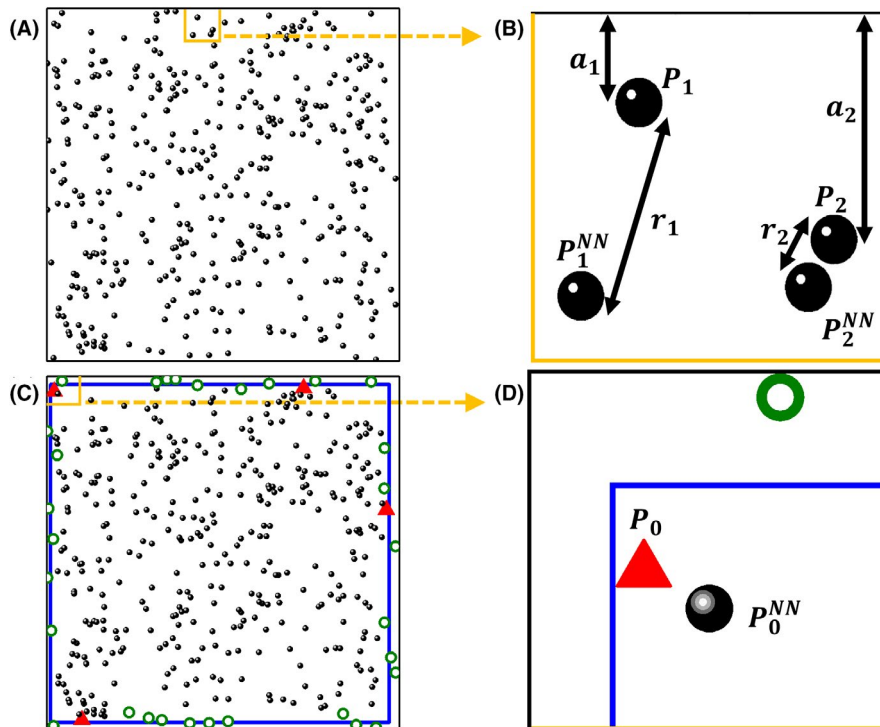

FIGURE 2 (A) Simulated random distribution of $N = 399$ points in a square unit-area. The inset represents the chosen area to illustrate the edge correction procedure. (B) The inset in (A) contains two particles P_1 and P_2 with their respective nearest neighbors P_1^{NN} and P_2^{NN}. According to the edge correction procedure, P_2 will be part of the new set of points while P_1 will be discarded. (C) After the edge correction, a new number of crystals $N' = 368$ was obtained, which are enclosed by a reduced area as indicated by the inner blue square. The discarded points are represented by open green circles and the outermost particles of the new distribution by red triangles. (D) The inset in (C) shows one of the four outermost points (P_0) taken as a reference to define the new area. The simulation was obtained with the Matplotlib[36] and the Scikit-learn[39] Python libraries

circle) and one of the discarded points (open green circle) after edge correction. The blue lines represent the edges of the new area.

Finally, with the new set of N' points and their respective Cartesian coordinates, the i-th nearest-neighbor distance (r_i) between a point P_i and its nearest-neighbor P_i^{NN} was obtained by calculating the shortest Euclidean distance

between every single point and the others, including the points filtered by the edge correction procedure. Although the discarded points are not taken into account in the calculation of N' and the new area, they are considered in the nearest-neighbor distances' calculations because they can be the nearest neighbors of nondiscarded points. Thus, parameter $\bar{r}$ was determined as the mean value of all the
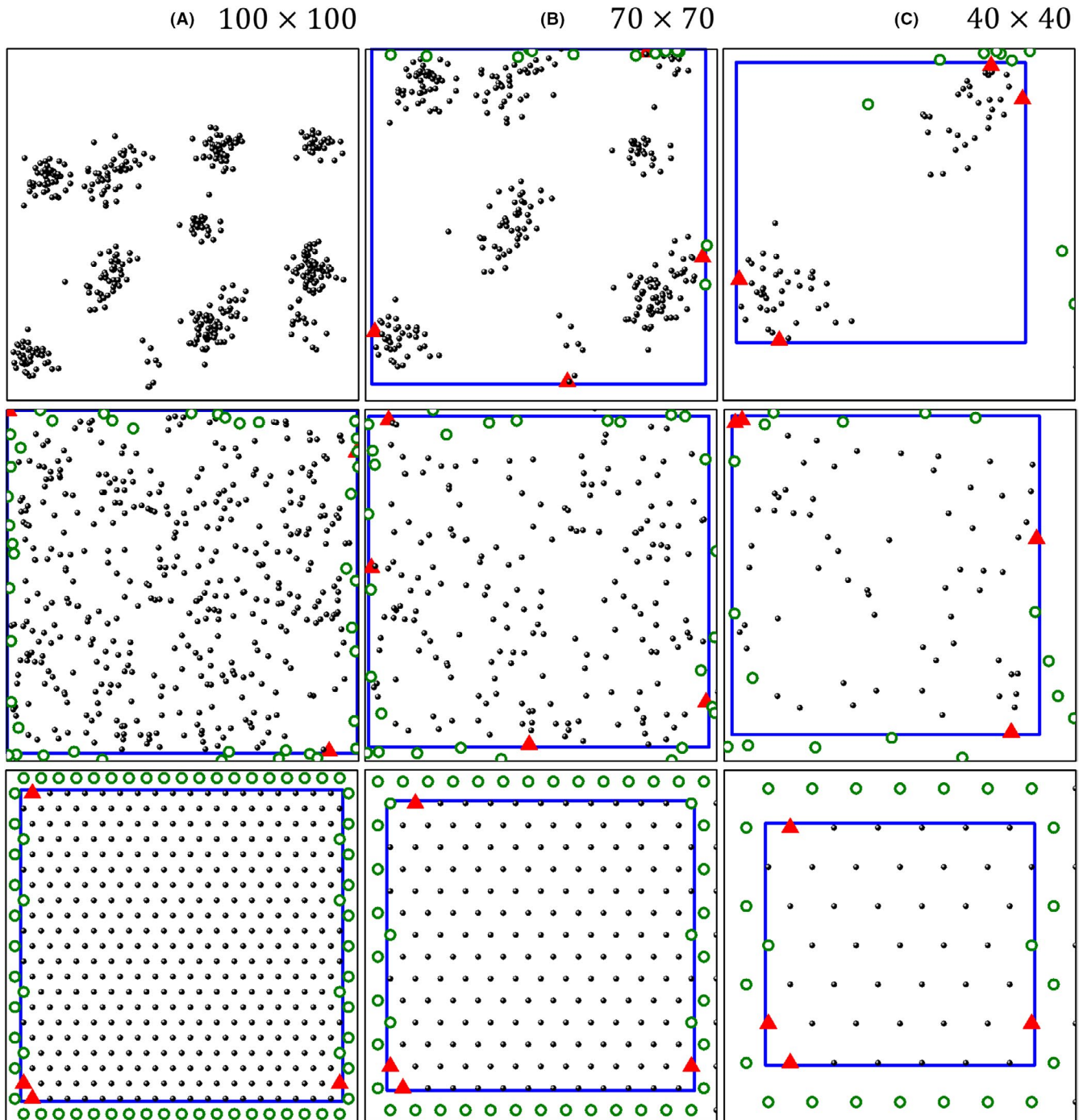

FIGURE 3 Simulated clustered (top), random (center), and hexagonal-periodic (bottom) distributions of points for three different arbitrary areas (in a.u.): (A) 100×100, (B) 70×70, and (C) 40×40. The total number of points for each distribution in the largest area is $N = 448$

nearest-neighbor distances, $\bar{r} = N'^{-1}\sum_i r_i$. Besides the determination of both the Cartesian coordinates of objects distributed in a 2D image and their nearest-neighbor distances is easily programmable in a computer routine, there are also free tools that can be used to accomplish this task in the ImageJ software.[37]

3.5 | Statistical significance

The statistical significance of the difference between $\bar{r}$ and $\bar{r}_E$ was determined via a two-tailed Z-score[38]:

$$Z = \frac{\bar{r} - \bar{r}_E}{\sigma_{\bar{r}_E}}. \tag{4}$$

The Z-score compares the mean nearest-neighbor distances of the observed and the expected random distributions, taking as reference the Poisson and the Weibull distribution characterized by $\bar{r}_E$ and $\sigma_{\bar{r}_E}$. Assuming a confidence level of 95%, two cases are considered:

- If $|Z| < 1.96$, the difference $\bar{r} - \bar{r}_E$ is not statistically significant, and we can say the observed distribution is random and homogeneous.
- If $|Z| \geq 1.96$, the difference $\bar{r} - \bar{r}_E$ is statistically significant, and the observed distribution of crystals departs from a uniform random and homogeneous distribution to a certain degree.

In the second case, the percentage of homogeneity can be accessed by taking the R-indexes for clustered, homogeneous, and periodic systems as $R_C = 0$, $R_H = 1$, and $R_P = 2.149$, respectively (see Section 2.3). If the experimental R-index (R) is less or greater than one, then the percentage of homogeneity can be calculated as: $\left[1 - \left(|R_H - R| / |R_H - R_i|\right)\right] 100\%$, with $i = C,P$. Hence, the R-index as defined by Equation (3) can be used as a good indicator to infer the homogeneity degree and determine an eventual tendency toward agglomeration or periodicity in 2D crystal distributions.

4 | RESULTS

4.1 | Simulated distributions

To test the validity of the edge correction procedure and the R-index (see Section 3.4), we considered the simulated distributions of points shown in Figure 1, which were created using the Matplotlib[36] and the Scikit-learn Python libraries.[39]

A population of $N = 448$ points was distributed in an area $A = 100 \times 100$ in arbitrary units (a.u.), following clustered, random and hexagonal-periodic configurations. From this

area, two other subareas equivalent to its 70% and 40% were outlined for each pattern, as presented in Figure 3A–C before (black margin) and after edge correction (blue margin). The values of N, N', A, ρ, $\bar{r}$, $\bar{r}_E$, R, var(R) and Z-score for the simulated distributions after edge correction are summarized in Table 2.

4.2 | Experimental crystal distributions

Figure 4A–C shows some representative optical micrographs acquired for the $Li_2Si_2O_5$ samples at three different magnifications, and two nucleation temperatures: 708 K (top) and 745 K (bottom). For both nucleation temperatures, the R-index was

TABLE 2 Values of N, N', A, ρ, $\bar{r}$, $\bar{r}_E$, R, var(R), and Z-score for the simulated distributions after edge correction

Distribution	Parameter	Results		
		100×100	70×70	40×40
Cluster	N	448	296	80
	N'	448	283	71
	A ($\times 10^3$ a.u.)	10	4.49	1.19
	ρ (a.u.)	0.04	0.06	0.06
	$\bar{r}$(a.u.)	1.16	1.16	1.07
	$\bar{r}_E$ (a.u.)	2.36	1.99	2.05
	R	0.49	0.58	0.52
	var (R) ($\times 10^{-4}$)	6.10	9.65	38.50
	Z	20.61	13.44	7.73
Random	N	448	220	82
	N'	405	192	65
	A ($\times 10^3$ a.u.)	9.74	4.51	1.34
	ρ (a.u.)	0.04	0.04	0.05
	$\bar{r}$(a.u.)	2.35	2.45	2.33
	$\bar{r}_E$ (a.u.)	2.45	2.42	2.27
	R	0.96	1.01	1.03
	var (R) ($\times 10^{-4}$)	6.75	14.20	42.00
	Z	1.58	0.27	0.41
Periodic	N	448	216	67
	N'	380	169	43
	A ($\times 10^3$ a.u.)	8.50	3.85	1.02
	ρ (a.u.)	0.04	0.04	0.04
	$\bar{r}$(a.u.)	5	5	5
	$\bar{r}_E$ (a.u.)	2.36	2.39	2.44
	R	2.12	2.09	2.05
	var (R) ($\times 10^{-4}$)	7.19	16.20	63.50
	Z	41.56	27.21	13.19

Note.: In this and other tables, some values must be <u>multiplied</u> by the factor within parentheses to obtain the actual quantity in its general form.

calculated for several micrographs (see Section 3.3) taken with 200×, 500×, and 1000× magnifications. The average values of N', A, ρ, $\bar{r}$, $\bar{r}_E$, R, var (R) and the Z-score for these micrographs, applying the edge correction, are summarized in Tables 3 and 4 for $T_n = 708$ K and 745 K, respectively.

Similarly, Figure 5A–C shows some representative optical micrographs for $Ba_5Si_8O_{21}$ samples, at two nucleation temperatures: 948 K (top) and 988 K (bottom). Since this composition presents spherical crystals, it is easier to obtain the Cartesian coordinates (x,y) of the crystals' geometric centers. In this case, the R-index was calculated considering the 500×, 1000×, and 1500× magnifications. The average values of N', A, ρ, $\bar{r}$, $\bar{r}_E$, R, var (R) and the Z-score for $Ba_5Si_8O_{21}$, with edge

correction, are summarized in Tables 5 and 6 for $T_n = 948$ K and 988 K, respectively.

5 | DISCUSSION

5.1 | Simulated distributions

The homogeneity degree of each simulated distribution (Figure 3) was initially evaluated by visual inspection and through the density of the points (ρ). As shown in Table 2, the simulated clustered distribution has a variable ρ ranging from 0.04 to 0.06 a.u., according to the size of the original
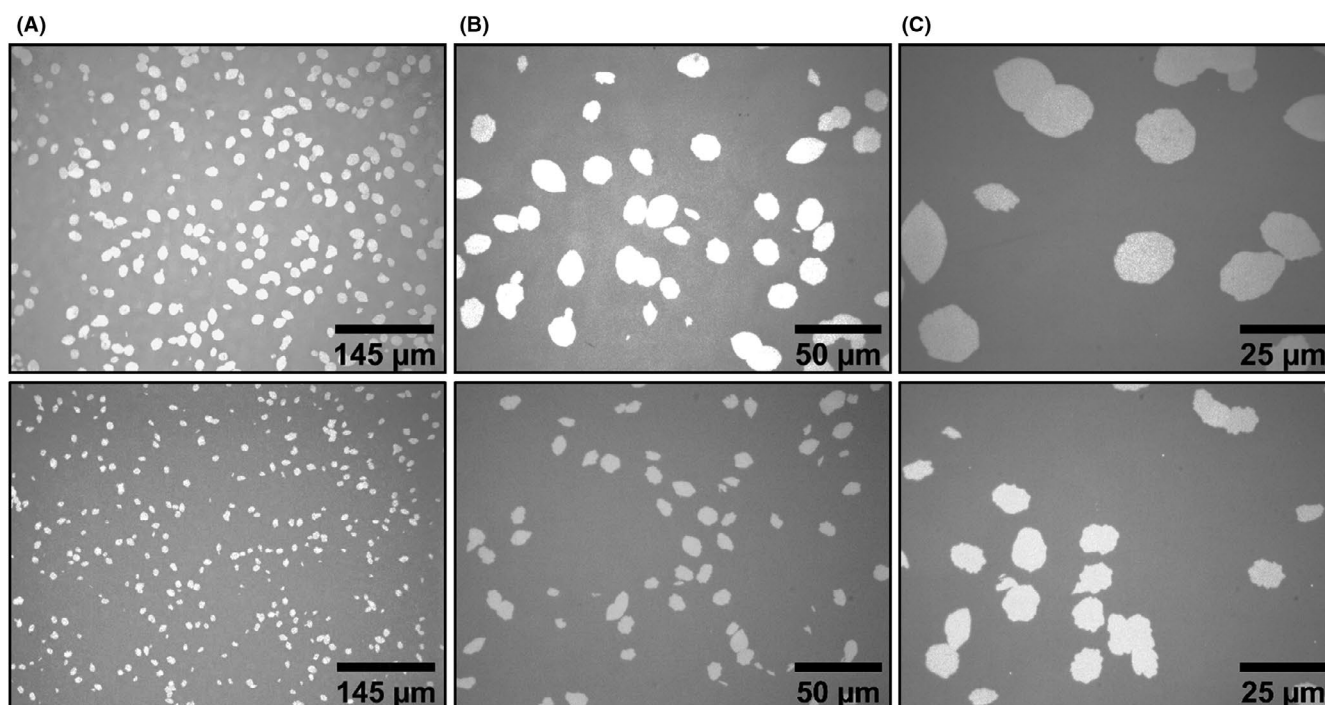

FIGURE 4 Optical micrographs for $Li_2Si_2O_5$ samples heat-treated at $T_n = 708$ K (top) for 63 h and at $T_n = 745$ K (bottom) for 7.5 h using the magnifications (A) 200×, (B) 500×, and (C) 1000×

TABLE 3 Average values of N', A, ρ, $\bar{r}$, $\bar{r}_E$, R, var (R), and Z-score for the experimental distributions of the $Li_2Si_2O_5$ crystals in the sample treated at $T_n = 708$ K for 63 h after edge correction

Parameters	$Li_2Si_2O_5$ ($T_n = 708$ K)					
	200×	Error	500×	Error	1000×	Error
N'	304	25	41	7	10	4
A ($\times 10^3$ μm^2)	291	4	40.60	1.88	8.46	0.80
ρ ($\times 10^{-3}$ μm^{-2})	1.05	0.10	1.01	0.22	1.18	0.58
$\bar{r}$ (μm)	15.75	0.68	14.61	1.60	13.11	2.62
$\bar{r}_E$ (μm)	15.50	0.67	15.95	1.18	15.19	3.09
R	1.02	0.09	0.92	0.17	0.86	0.35
var (R) ($\times 10^{-4}$)	9.04		69.00		313	
Z	0.53		1.03		0.89	

TABLE 4 Average values of N', A, ρ, $\bar{r}$, $\bar{r}_E$, R, var (R), and Z-score for the experimental distributions of the $Li_2Si_2O_5$ crystals in the sample treated at $T_n = 745$ K for 7.5 h after edge correction

Parameters	$Li_2Si_2O_5$ ($T_n = 745$ K)					
	200×	Error	500×	Error	1000×	Error
N'	281	14	38	5	8	3
A ($\times 10^3$ μm²)	283	3	36.70	1.53	5.86	1.42
ρ ($\times 10^{-3}$ μm⁻²)	0.99	0.06	1.04	0.18	1.36	0.84
$\bar{r}$ (μm)	16.75	0.88	15.27	1.37	12.89	3.07
$\bar{r}_E$ (μm)	15.88	0.40	15.63	0.95	14.36	3.25
R	1.05	0.08	0.98	0.15	0.90	0.42
var (R) ($\times 10^{-4}$)	9.75		73.20		434	
Z	1.75		0.28		0.58	

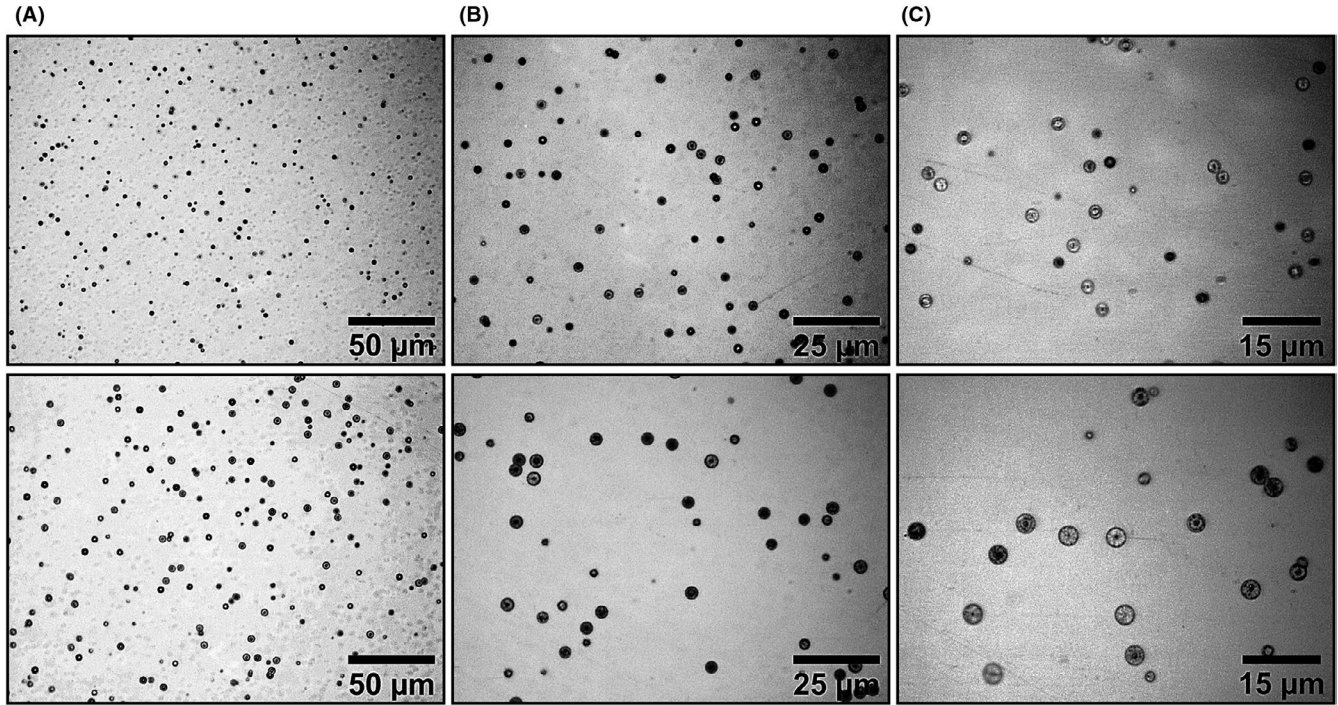**FIGURE 5** Optical micrographs for the $Ba_5Si_8O_{21}$ samples heat-treated at $T_n = 948$ K (top) for 5 h and at $T_n = 988$ K (bottom) for 10 min using the magnifications (A) 500×, (B) 1000×, and (C) 1500×

TABLE 5 Average values of N', A, ρ, $\bar{r}$, $\bar{r}_E$, R, var (R) and Z-score for the experimental distributions of the $Ba_5Si_8O_{21}$ crystals in the sample treated at $T_n = 948$ K for 5 h after edge correction

Parameters	$Ba_5Si_8O_{21}$ ($T_n = 948$ K)					
	500×	Error	1000×	Error	1500×	Error
N'	232	18	51	7	20	6
A ($\times 10^3$ μm²)	43.40	0.67	9.56	0.42	3.50	0.35
ρ ($\times 10^{-3}$ μm⁻²)	5.34	0.50	5.33	0.97	5.71	2.29
$\bar{r}$ (μm)	6.61	0.27	6.37	0.72	6.28	1.01
$\bar{r}_E$ (μm)	6.85	0.24	6.90	0.40	6.80	0.73
R	0.96	0.07	0.92	0.16	0.92	0.25
var (R) ($\times 10^{-4}$)	11.80		54.90		148	
Z	1.04		1.06		1.16	

observation area. This result, in addition to the precise disposition of points at preferential sites, is a sign of heterogeneity in the clustered system (see Section 2.2). It is worth mentioning that the 100×100 a.u. cluster distribution is still the same before and after the edge correction since, in this case, the distance of all the crystals to their nearest-neighbors

Parameters	Ba$_5$Si$_8$O$_{21}$ (T_n = 988 K)					
	500×	Error	1000×	Error	1500×	Error
N'	172	13	40	7	14	4
A (×10^3 μm^2)	42.50	0.98	9.10	0.72	3.02	0.52
P (×10^{-3} μm^{-2})	4.04	0.40	4.39	1.12	4.64	2.12
$\bar{r}$(μm)	7.63	0.51	7.17	0.88	7.29	1.35
$\bar{r}_E$ (μm)	7.88	0.31	7.65	0.56	7.58	0.82
R	0.97	0.10	0.94	0.18	0.96	0.28
var (R) (×10^{-4})	16.00		71.40		219	
Z	0.79		0.76		0.28	

TABLE 6 Average values of N', A, ρ, $\bar{r}$, $\bar{r}_E$, R, var (R) and Z-score for the experimental distributions of the Ba$_5$Si$_8$O$_{21}$ crystals in the sample treated at T_n = 988 K for 10 min after edge correction

is smaller than their distance to one of the analyzed area edges, and therefore, $N' = N$.

The periodic distribution is also heterogeneous, despite having a constant $\rho = 0.04$ a.u. for all the studied areas. The privileged location of points at linear regions (columns and rows) indicates such heterogeneity. On the other hand, the simulated random distribution, characterized by a nearly constant density $\rho \sim 0.04$ a.u. at the different areas, along with a random disposition of points, suggests a highly homogeneous distribution.

Although the qualitative analysis exposed above can be used as a first approximation to verify the point distribution behavior, a more precise quantification is given by the R-index, presented in Table 2. Therein, $R = 0.49, 0.58,$ and 0.52 for the cluster distribution, and $R = 2.12, 2.09,$ and 2.05 for the periodic distribution at the evaluated unit area and subareas confirm a tendency of these patterns towards agglomeration and periodicity, respectively. The R-index for the simulated periodic point distribution is close to, but not exactly equal to 2.149 since, in this case, the point distribution is embedded inside a square area instead of a hexagonal one. In turn, the aggregation index is $R = 0.96, 1.01$ and 1.03 (close to the theoretical value 1.00) for the random point distribution, indicating its uniform, random nature.

Since the simulated clustered and periodic distributions have a Z-score much greater than 1.96 (see Section 3.5), both depart from the homogeneous, uniform random expectation, with a high statistical significance. As these distributions are neither perfectly agglomerated nor perfectly periodic, they have a certain degree or percentage of homogeneity, which correspond to ~49%, 58%, and 52% for the agglomerated patterns and ~3%, 5%, and 9% for the periodic ones. For the simulated cluster distribution, the percentage of homogeneity was very high because despite the fact that the clusters are evident, there are local homogeneities in the distribution of points inside them. On the other hand, the percentage of homogeneity for the simulated periodic point distributions is low, since the only thing that prevents them from reaching $R = 2.149$ is that they are within a square instead of a hexagonal area.

The opposite occurs for the simulated random distribution, with a Z-score smaller than 1.96, meaning that the departure from uniform random and homogeneous expectation is not statistically significant. According to these analyses, the simulated patterns are good representations of clustered, uniform random, and periodic point distributions for the different selected areas. They also serve as a practical example validating the use of the R-index in the determination of the homogeneity degree, the associated scale, and the tendency towards agglomeration, uniform randomness, or periodicity of crystal distribution in a 2D space.

5.2 | Experimental crystal distributions

An important question that arises in studies of crystallization in glasses that undergo internal nucleation is whether completely homogeneous nucleation can occur.[18] Due to the apparent random disposition of the crystals in the vitreous matrix, even a cursory visual inspection of the Li$_2$Si$_2$O$_5$ and Ba$_5$Si$_8$O$_{21}$ crystal distributions in optical micrographs similar to those shown in Figures 4 and 5 suggests a high chemical homogeneity degree at the different analyzed magnifications (200×, 500×, 1000×, and 1500×). A constant ρ, within the experimental error (Tables 3-6), is also an indication of homogeneity. Nevertheless, small departures from the perfect homogeneity cannot be discriminated by the bare eye, validating quantification methods such as the R-index.

For both systems, the R-index is close to 1, ranging from 0.86 to 1.05 for Li$_2$Si$_2$O$_5$ glass and from 0.92 to 0.97 for Ba$_5$Si$_8$O$_{21}$ glass, depending on the micrograph magnification. However, if the errors are taken into account, all these values are close to 1. Hence, these results indicate that the experimental distribution is indeed uniform, and this homogeneity is not significantly distinct in different scales, as seen by the different magnifications used. The reliability of these results is sustained by the Z-scores lower than the critical value of 1.96. Therefore, the crystal distributions are statistically equal to a perfect homogenous distribution, suggesting

complete spatial uniform randomness and the parent glasses' chemical homogeneity.

It is worth mentioning that, even though our analysis was carried out in a 2D space, the present conclusions are valid for the crystal distribution in a 3D glass matrix since the observed bidimensional distributions are statistically representative samples of the system as a whole. Hence, any chemical inhomogeneity existing in the glass volume (3D) would be detected by our 2D analysis because the micrographs are simply cross-sections through the material's interior. An alternative analysis could be carried out by determining the 3D *R*-index directly if the experimental conditions allow it,[40] for instance using transmitted light microscopy, or by inferring it from the 2D analysis employing a stereological correction. This type of correction permits calculating the volumetric crystal number density from the observed number in samples' cross-sections.[30]

Additionally, the results indicate that the implemented method of crushing and remelting the glass more than once can lead to chemically homogeneous samples. Nevertheless, there are other cases involving glasses having low melt viscosity where the chemical homogeneity is already achieved with the first cycle and is not improved by increasing the number of crushing and remelting cycles.[12]

Finally, the current results show no evidence for the hypothesis of crystal clustering, local heterogeneities that would be induced by an eventual formation of satellite-like crystals near previously existing ones, as suggested in a billion-atom molecular dynamic simulation of homogeneous nucleation in supercooled iron melt.[18]

6 | SUMMARY

We tested a statistical method (*R*-index) to characterize the spatial crystal distribution and the associated degree of chemical homogeneity of partially crystalized glasses using $Li_2Si_2O_5$ and $Ba_5Si_8O_{21}$ as model materials. We found an *R*-index close to 1 for both glass-ceramics in all analyzed areas, showing that the crystals are uniformly and randomly distributed, corroborating the concept that nucleation is indeed a stochastic process.

Our results also confirm that the experimental method used for glass production at laboratory scale—melting/crushing/remelting a few times—can lead to chemically homogeneous samples.

Finally, as none of the crystal distributions showed a tendency towards agglomeration, we *deny* the hypothesis of the preferential formation of satellite-like crystals near previously existing ones, that is, the nucleation self-correlation conundrum.

On the whole, these results validate the *R*-index as an efficient parameter to evaluate the chemical homogeneity of glasses that undergo internal crystal nucleation, such as those used for glass-ceramic production.

ORCID

María Helena Ramírez Acosta https://orcid.org/0000-0001-6023-1693
Lorena Raphael Rodrigues https://orcid.org/0000-0002-7270-6040
Edgar David Guarin Castro https://orcid.org/0000-0002-5226-1945
Edgar Dutra Zanotto https://orcid.org/0000-0003-4931-4505

REFERENCES

1. Afghan M, Cable M. Estimation of the homogeneity of glass by the Christiansen filter method. J Non Cryst Solids. 1980;38:3–8.
2. Varshneya AK. Glass homogeneity measurement using Shelyubskii technique. J Non Cryst Solids. 1986;80(1–3):688–92.
3. Jensen M, Zhang L, Keding R, Yue Y. Homogeneity of inorganic glasses: Quantification and ranking. Int J Appl Glas Sci. 2011;2(2):137–43.
4. Yildiz T, Günay V, Ariburnu D. Determination of the homogeneity factors of industrial container glasses by the Christiansen-Shelyubskii method. J Chem Technol Metall. 2015;50(4):397–403.
5. Unnikrishnan VK, Nayak R, Kartha VB, Santhosh C, Sonavane MS, Yeotikar RG, et al. Homogeneity testing and quantitative analysis of manganese (Mn) in vitrified Mn-doped glasses by laser-induced breakdown spectroscopy (LIBS). AIP Adv. 2014;4(9):97104.
6. Castro JP, Gallo LS, Zanotto ED, Pereira-Filho ER. Glass and glass-ceramic homogeneity evaluation using laser ablation inductively coupled plasma mass spectrometry (LA-ICP-MS). Brazilian J Anal Chem. 2017;4(15):8–18.
7. Hoffmann H-J, Steinhart R. Spectral transmittance of Christiansen filters-Experimental observations. Glas Sci Technol. 1998;71(11):319–26.
8. Hoffmann H-J. Theory of the spectral transmittance of Christiansen filters. Glas Sci Technol. 2003;76(6):285–97.
9. Costa VC, Castro JP, Andrade DF, Victor Babos D, Garcia JA, Speran ça MA, et al. Laser-induced breakdown spectroscopy (LIBS) applications in the chemical analysis of waste electrical and electronic equipment (WEEE). TrAC - Trends Anal Chem. 2018;108:65–73.
10. Tooley FV, Tiede RL. Factors affecting the degree of homogeneity of glass. J Am Ceram Soc. 1944;27(2):42–5.
11. Krasheninnikova NS, Frolova IV, Kaz'mina OV. A method for preparing homogeneous glass batch. Glas Ceram. 2004;61(5–6):173–4.

12. Souza LA, Leite MLG, Zanotto ED, Prado MO. Crystallization statistics. A new tool to evaluate glass homogeneity. J Non Cryst Solids. 2005;351(46–48):3579–86.

13. Lumeau J, Sinitskii A, Glebova L, Glebov LB, Zanotto ED. Method to assess the homogeneity of partially crystallized glasses: Application to a photo-thermo-refractive glass. J Non Cryst Solids. 2009;355(34–36):1760–8.

14. Chopinet M-H, Gouillart E, Papin S, Toplis MJ. Influence of limestone grain size on glass homogeneity. Glas Technol J Glas Sci Technol Part A. 2010;51(3):116–22.

15. Bartolomey S, Krogel S, Conradt R, Roos C. Quantification of the thermal and chemical inhomogeneity of glasses. Int J Appl Glas Sci. 2018;9(1):16–23.

16. Baddeley A, Rubak E, Turner R. Spatial Point Patterns: Methodology and Applications with R. Boca Raton, FL: CRC Press; 2015.

17. Clark PJ, Evans FC. Distance to nearest neighbor as a measure of spatial relationships in populations. Ecol. 1954;35(4):445–53.

18. Shibuta Y, Sakane S, Miyoshi E, Okita S, Takaki T, Ohno M. Heterogeneity in homogeneous nucleation from billion-atom molecular dynamics simulation of solidification of pure metal. Nat Commun. 2017;8(1):1–9.

19. Illian J, Penttinen A, Stoyan H, Stoyan D. Statistical analysis and modelling of spatial point patterns, vol. 70. Chichester: John Wiley & Sons; 2008.

20. Bhattacharya RN, Waymire EC. Stochastic processes with applications. SIAM. 2009.

21. Kelton KF, Greer AL. Nucleation in Condensed Matter: Applications in Materials and Biology, vol. 15. Oxford: Elsevier; 2010.

22. Zanotto ED, Mauro JC. The glassy state of matter: Its definition and ultimate fate. J Non Cryst Solids. 2017;471:490–5.

23. Müller R, Zanotto ED, Fokin VM. Surface crystallization of silicate glasses: Nucleation sites and kinetics. J Non Cryst Solids. 2000;274(1):208–31.

24. Komatsu T, Honma T. Nucleation and crystal growth in laser-patterned lines in glasses. Front Mater. 2016;3:32.

25. Fokin VM, Souza GP, Zanotto ED, Lumeau J, Glebova L, Glebov LB. Sodium fluoride solubility and crystallization in photo-thermo-refractive glass. J Am Ceram Soc. 2010;93(3):716–21.

26. Dyamant I, Abyzov AS, Fokin VM, Zanotto ED, Lumeau J, Glebova LN, et al. Crystal nucleation and growth kinetics of NaF in photo-thermo-refractive glass. J Non Cryst Solids. 2013;378:115–20.

27. Hertz P. Über den gegenseitigen durchschnittlichen Abstand von Punkten, die mit bekannter mittlerer Dichte im Raume angeordnet sind. Math Ann. 1909;67(3):387–98.

28. Petrere M. The variance of the index (R) of aggregation of Clark and Evans. Oecologia. 1985;68(1):158–9.

29. Deubener J, Montazerian M, Krüger S, Peitl O, Zanotto ED. Heating rate effects in time-dependent homogeneous nucleation in glasses. J Non Cryst Solids. 2017;474:1–8.

30. Fokin VM, Zanotto ED, Yuritsyn NS, Schmelzer JWP. Homogeneous crystal nucleation in silicate glasses: a 40 years perspective. J Non Cryst Solids. 2006;352(26–27):2681–714.

31. Xia X, Van HDC, Mckenzie ME, Youngman RE, Gulbiten O, Kelton KF. Time-dependent nucleation rate measurements in BaO·2SiO$_2$ and 5BaO·8SiO$_2$ glasses. J Non Cryst Solids. 2019;525:119575.

32. Xia X, Van Hoesen DC, McKenzie ME, Youngman RE, Kelton KF. Low-temperature nucleation anomaly in silicate glasses shown to be artifact in a 5BaO·8SiO$_2$ glass. Nat Commun. 2021;12(2026):1–6.

33. Sample size calculators. 2020. Available from: https://www.statskingdom.com/sample_size_all.html

34. Schneider CA, Rasband WS, Eliceiri KW. NIH Image to ImageJ: 25 years of image analysis. Nat Methods. 2012;9(7):671–5.

35. Pommerening A, Stoyan D. Edge-correction needs in estimating indices of spatial forest structure. Can J For Res. 2006;36(7):1723–39.

36. Hunter JD. Matplotlib: A 2D graphics environment. Comput Sci Eng. 2007;9(3):90–5.

37. Mao Y. Nearest neighbor distances calculation with ImageJ. 2016. Available from: https://icme.hpc.msstate.edu/mediawiki/index.php/Nearest_Neighbor_Distances_Calculation_with_ImageJ.html

38. Bernstein S, Bernstein R. Schaum's Outline of Elements of Statistics II: Inferential Statistics. 1st edn. New York: McGraw-Hill Education; 1999:350–461.

39. Pedregosa F, Varoquaux G, Gramfort A, Michel V, Thirion B, Grisel O, et al. Scikit-learn: Machine learning in Python. J Mach Learn Res. 2011;12:2825–30.

40. Clark PJ, Evans FC. Generalization of a nearest neighbor measure of dispersion for use in K dimensions. Ecol. 1979;60(2):316–7.